# Electronic Supplementary Information (ESI)

## Hierarchical porous carbon sheets for high-performance room temperature sodium-sulfur batteries: integration of Nitrogen-self-doping and space confinement

Jirong Mou[a], Ting Liu[a], Yijuan Li[a], Wenjia Zhang[a], Mei Li[a], Yuting Xu[a], Jianlin Huang*[a], and Meilin Liu[b]

[a]Guangzhou Key Laboratory for Surface Chemistry of Energy Materials, New Energy Research Institute, School of Environment and Energy, South China University of Technology, Guangzhou 510006, China.

[b]School of Materials Science & Engineering, Georgia Institute of Technology, Atlanta, GA 30332-0245, USA.

* Corresponding authors.

E-mail: jianlinhuang@scut.edu.cn

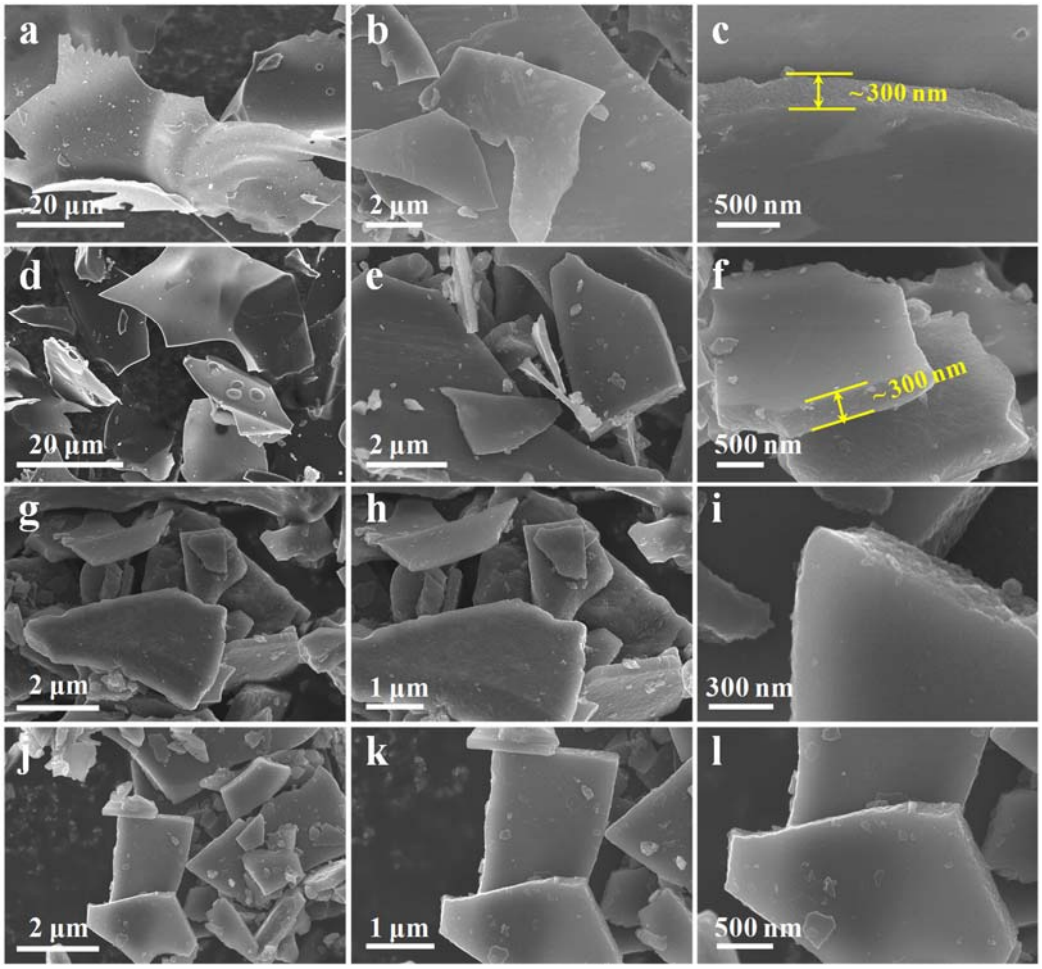


**Fig. S1**. The SEM images of NPC-650 (a-c), NPC-750 (d-f), S@NPC-650 (g-i), and S@NPC-750 (j-l), respectively.

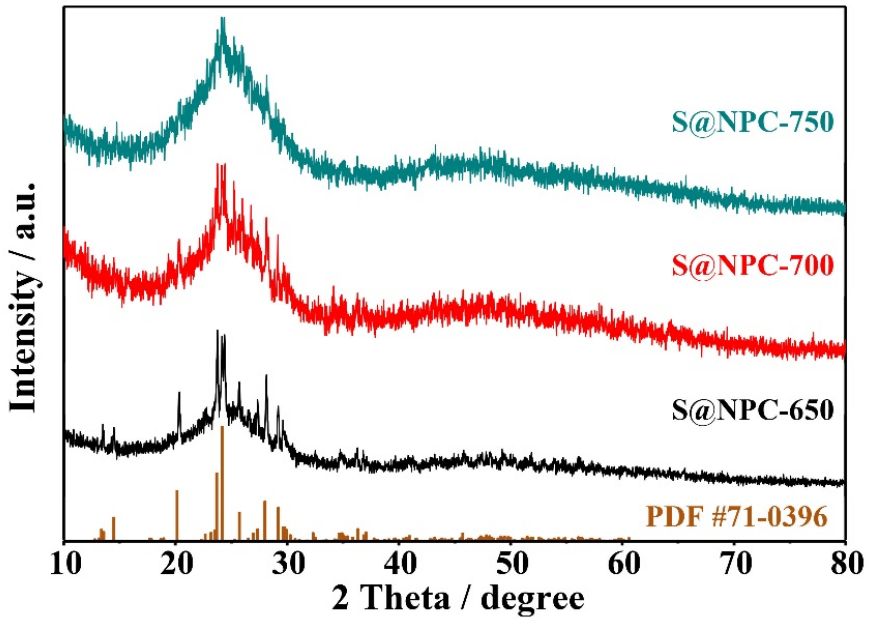


**Fig. S2**. XRD patterns of S@NPC with different temperature.

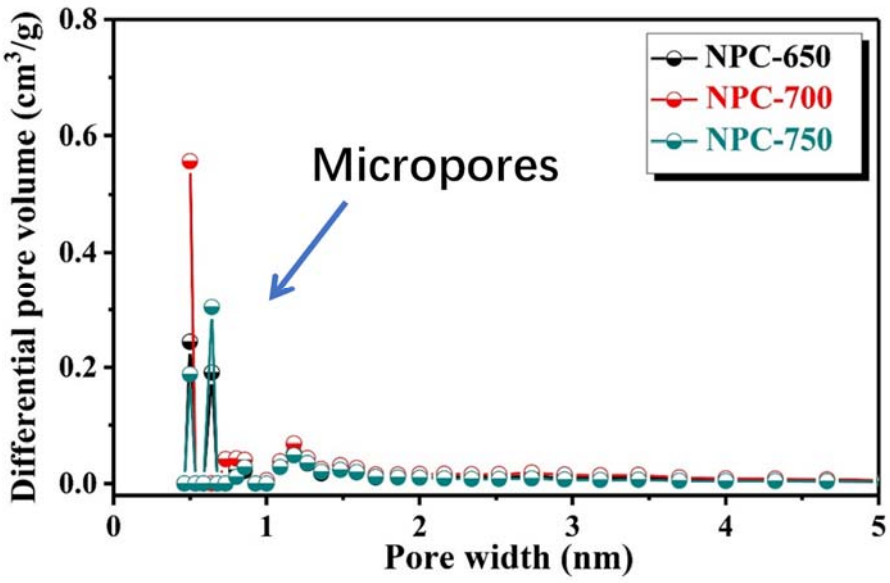


**Fig. S3.** The pore distribution curves of the as-prepared NPC with different temperature.

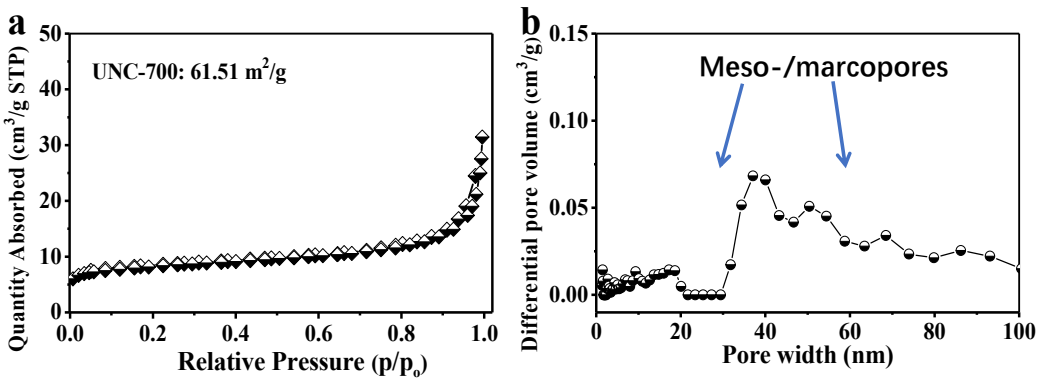


**Fig. S4**. (a) $N_2$ adsorption-desorption isotherms and (b) The pore distribution curves of UNC-700.

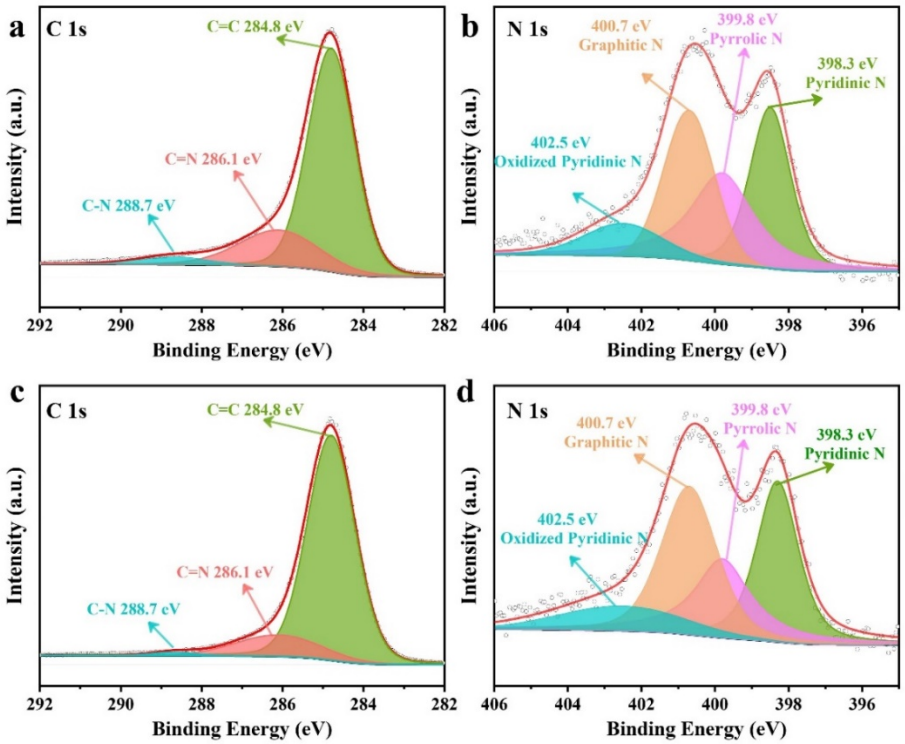


**Fig. S5.** The high-resolution XPS spectra of C 1s and N 1s for (a-b) NPC-650 and (c-d) NPC-750, respectively.

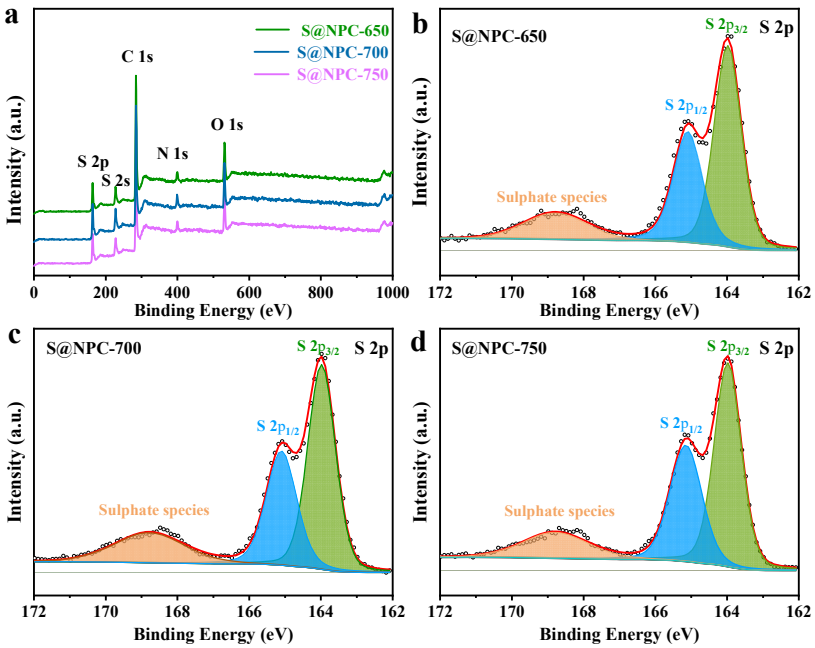


**Fig. S6.** The XPS survey spectrum of S@NPC composites (a), and the high-resolution S 2p of S@NPC-650 (b), S@NPC-700 (c), and S@NPC-650 composites (d).

***Note:*** As shown in Fig.S6, peaks of C, N, O and S elements are observed in three S@NPC samples, with no other impurities detected. In S 2p XPS spectrum, the S 2p spectra show a S $2p_{3/2}$ peak locating at 163.9 eV and a S $2p_{1/2}$ peak at 165.1 eV, corresponding to S-S bonds.[S9] Besides, a small broad peak appeared at 168.8 eV, which is ascribed to the sulfate species formed by partial oxidation of sulfur in air and C-S chemical bonds.[S10,S11] Thus, the XPS data indicate that the sulfur is successfully introduced into carbon sheet host. Moreover, the doping of these electron-rich heteroatoms, i.e., O and N, could produce abundant active sites and tune the surface electronic structure of the carbon materials, thus promoting the surface affinity for polysulfides.[43,49,S12]

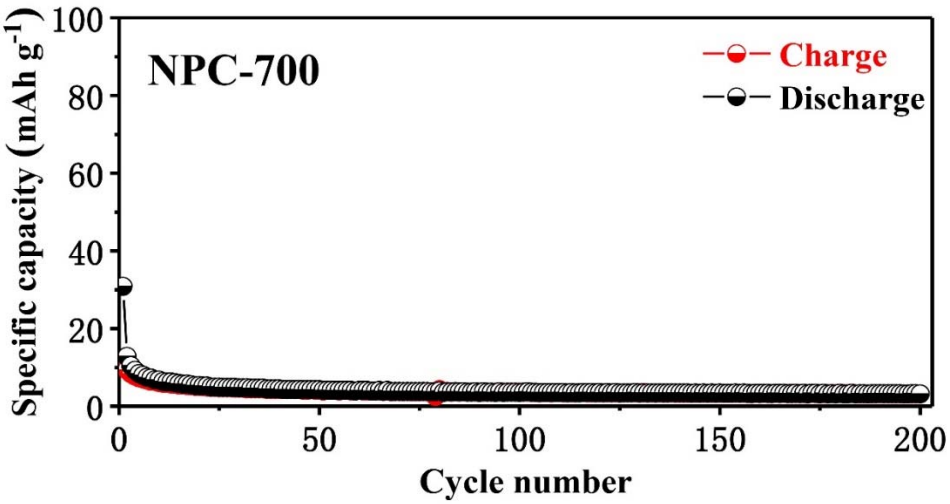


**Fig. S7.** Cycling performance of the NPC-700 at 0.1 C.

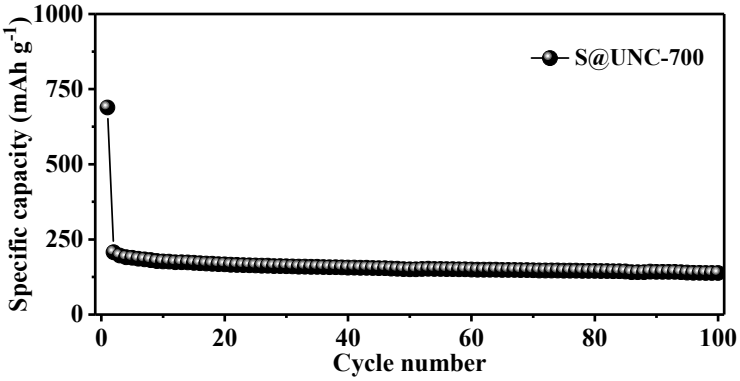


**Fig. S8.** The cyclic performance of S@UNC-700 at 0.1 C.

***Note:*** The nitrogen doped carbon material, without addition of $ZnCl_2$, was synthesized by the same process at 700 ºC and denoted as UNC-700. As shown in Fig. S4, the UNC-700 displayed a representative II isotherms, implying the coexistence of mesopores and macropores (Fig.S4b). The specific surface area of UNC-700 is 61.5 $m^2$ $g^{-1}$, which is much smaller than that of NPC-700 (918 $m^2$ $g^{-1}$). These results indicate that $ZnCl_2$ has facilitated the creation of more micro-/nanopores in carbon sheets, as confirmed by pore size distribution (Fig. 3c and Fig. S3). Besides, the S@UNPC cathode of RT Na-S battery was also tested under the same conditions and showed a very low specific capacity of 207 mA h $g^{-1}$ at 0.1C (Fig. S8) compared to S@NPC-700 (725.5 mA h $g^{-1}$), suggesting the introduction of the micro-/nanoporous sheet structure in the S@NPC-700 can significantly improve electrochemical activities of RT Na-S battery.

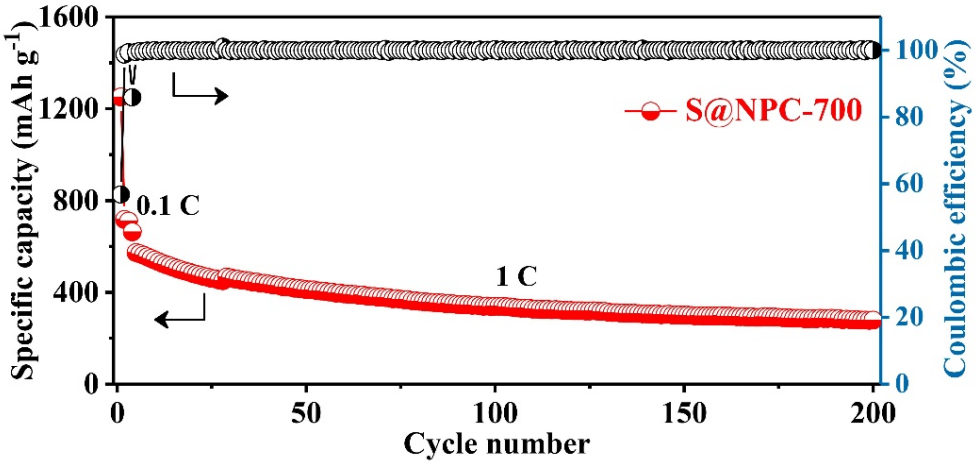


**Fig. S9.** Cycling performance of the S@NPC-700 at 1.0 C.

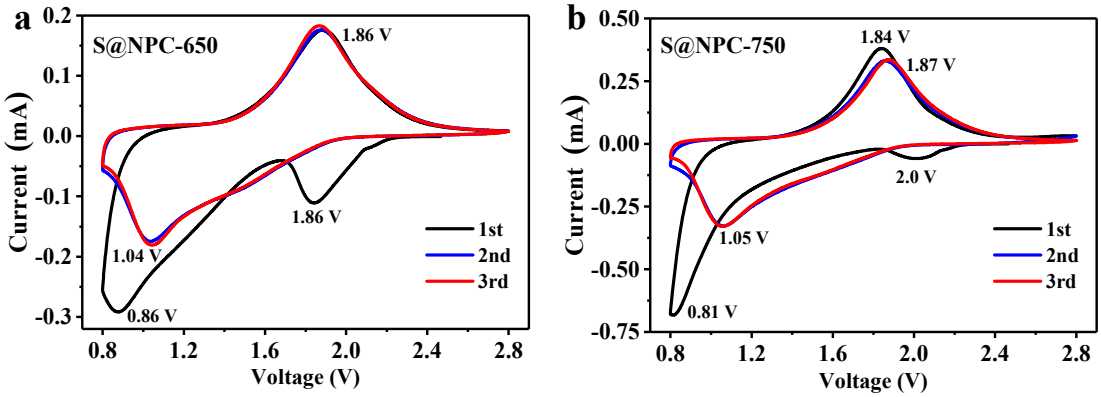


**Fig. S10**. The CV curves of S@NPC-650 (a) and S@NPC-750 (b) at 0.1 mV/s.

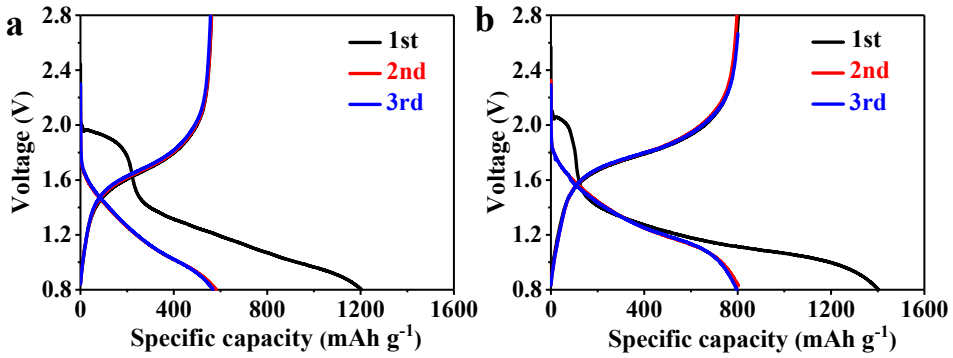


**Fig. S11.** The discharge/charge profiles of S@NPC-650 (a) and S@NPC-750 (b) cathodes at 0.1 C.

***Note:*** Similar CV behaviors are observed for the S@NPC-650, S@NPC-700 and S@NPC-750 (Fig. 5a, and Fig.S10). Notably, the potential difference of S@NPC-700 (0.79 V) is smaller than those of S@NPC-650 (0.82 V) and S@NPC-750 (0.82 V) in the 2nd and 3rd cycles, indicating smaller potential polarization for S@NPC-700. Compared with S@NPC-650 and S@NPC-750 cathodes, the CV curves of S@NPC-700 cathode show greater reproducibility after the initial cycle, implying better cycling stability and reversibility. As Fig. 5b and Fig. S11 show the discharge/charge profiles of the S@NPC cathodes at 0.1 C. In the initial discharge/charge profiles of the S@NPC cathodes at 0.1 C (Fig. S11), two plateaus were observed in the voltage ranges of 2.0-1.8 V and 1.65-0.8 V. In the subsequent discharge processes, however, the high-voltage plateau disappeared, which is consistent with the CV results.

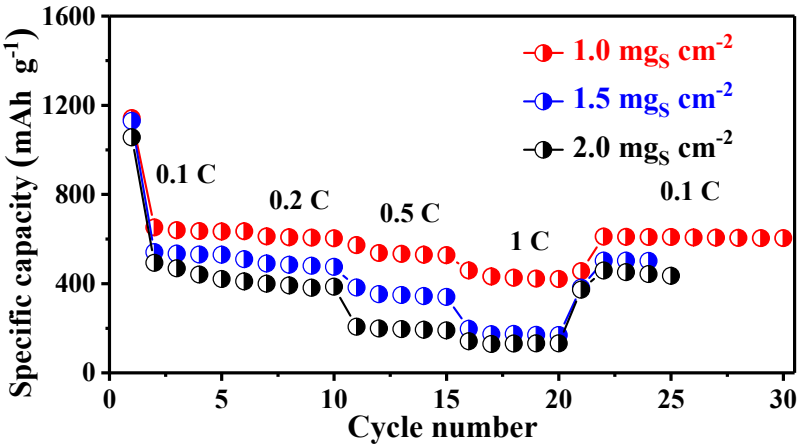


**Fig. S12.** The rate performance of S@NPC-700 from 0.1 to1.0 C with different areal sulfur loadings (1.0, 1.5 and 2.0 mg $cm^{-2}$).

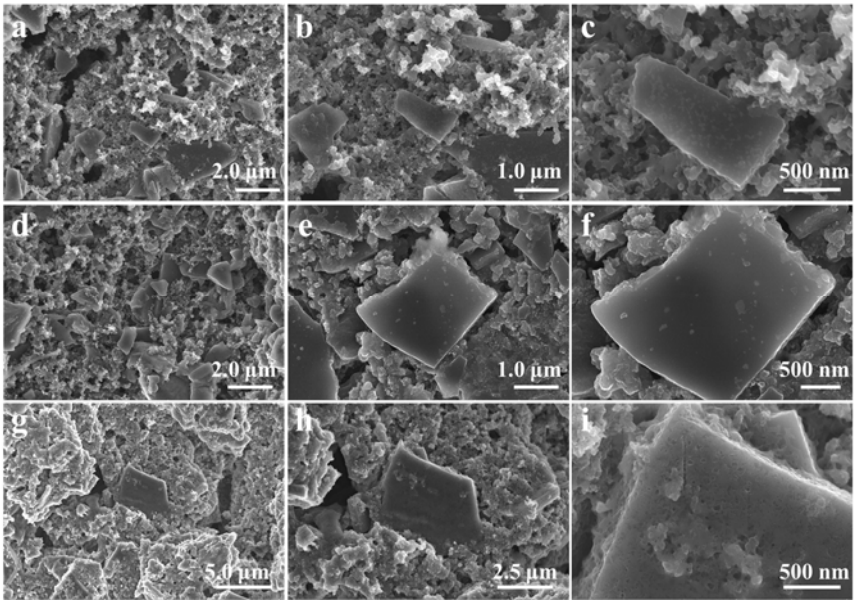


**Fig. S13.** FESEM images of S@NPC-650 (a-c), S@NPC-700 (d-f), and S@NPC-750 (g-i) for after 200 cycles at 1.0 C.

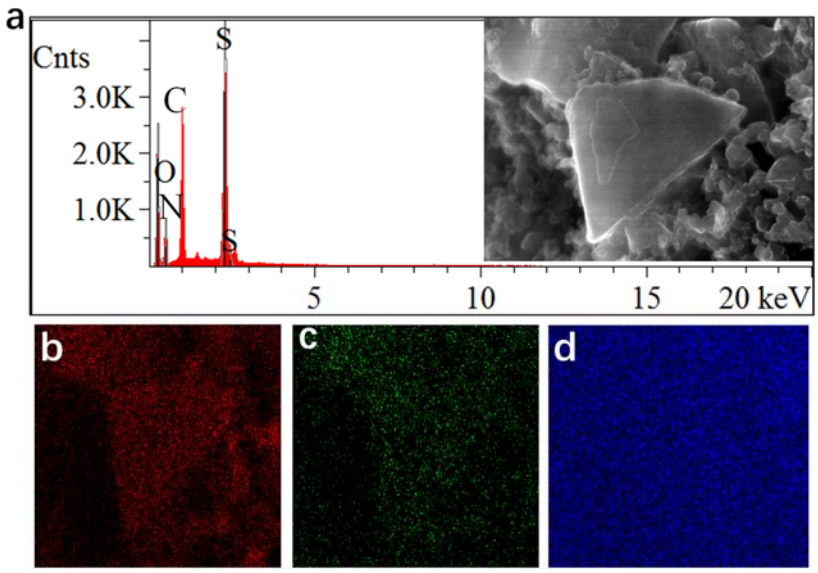


**Fig. S14.** FESEM images of S@NPC-700 at 1.0 C after 200 cycles, and (b-d) corresponding elemental mapping images of C, O and S, respectively.

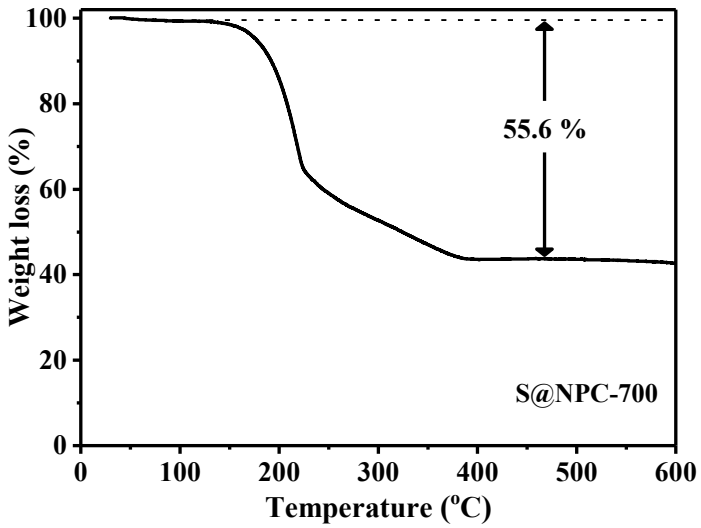


**Fig. S15.** TGA curves of S@NPC-700 with a sulfur loading of 55.6 wt%.

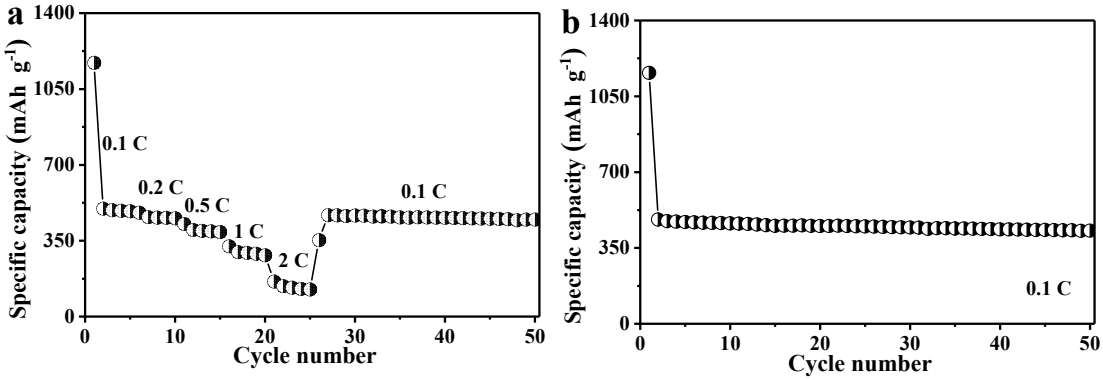


**Fig. S16.** (a) rate performance and (b) Cycling performance at 0.1 C for the S@NPC-700 with a sulfur loading of 55.6%.

***Note*:** However, the sulfur loading is in the range of 40-60 wt% for most of RT Na-S batteries.[S1,S4,S7] As suggested, the S@NPC-700 electrode with a sulfur loading of 55.6 wt% was further synthesized by increasing the ratio of S/C in the precursors (Fig. S15). However, the specific capacity at 2.0 C rate decreased to 162.2 mAh $g^{-1}$ when the sulfur mass loading was increased to 55.6 wt% (Fig. S16a). The decrease in specific capacity with the increase in sulfur mass loading is attributed likely to ineffective sulfur utilization associated with poor charge and mass transfer. Meanwhile, the S@NPC-700 cathode with sulfur loading of 55.6 wt% showed no obvious capacity decay for 50 cycles, delivering a specific capacity of 428.6 mAh $g^{-1}$ at 0.1 C, (Fig. S16b).

**Table S1**. Microstructural properties of the samples studied

| Sample | BET surface area ($m^2/g$) | Pore volume ($cm^3/g$) | Pore size range (nm) |
|---|---|---|---|
| NPC-650 | 685 | 0.328 | 0.5-1.5 |
| NPC-700 | 918 | 0.439 | 0.5-1.5 |
| NPC-750 | 731 | 0.338 | 0.5-1.5 |
| UNC-700 | 61.5 | 0.0786 | 30-80 |

***Note:*** The porous structural parameters of the NPC sheets have been provided in Table. S1. The specific surface area and the total pore volume of the samples, as estimated from $N_2$ adsorption/desorption isotherms (Fig. 3c, and Fig. S4), are 685 $m^2\ g^{-1}$/0.328 $cm^3\ g^{-1}$ for the NPC-650, 918 $m^2\ g^{-1}$/0.439 $cm^3\ g^{-1}$ for the NPC-700, 731 $m^2\ g^{-1}$/0.338 $cm^3\ g^{-1}$ for the NPC-750, and 61.5 $m^2\ g^{-1}$/0.0786 $cm^3\ g^{-1}$ for the UNC-700 composites, respectively. As is well known, the BET specific surface area, pore volume and pore size of NPC samples depend sensitively on the synthesis conditions, thus altering the performance of the NPC cathodes in RT Na-S batteries.

**Table S2.** Elemental content of N species in NPC samples with different temperature.

| N 1s | Pyridinic-N (at%) | Pyrrolic-N (at%) | Graphitic -N (at%) | Oxidized-N (at%) | N species total content (at%) |
|---|---|---|---|---|---|
| NPC-650 | 29.56 | 30.79 | 28.94 | 10.71 | 3.14 |
| NPC-700 | 33.19 | 25.64 | 30.48 | 10.69 | 5.5 |
| NPC-750 | 30.31 | 23.48 | 34.85 | 11.36 | 3.67 |

**Table S3.** Impedance parameters simulated from the equivalent circuits.

| Cathodes | $R_s$ (Ω) | $R_{ct}$ (Ω) |
|---|---|---|
| S@NPC-650 | 8.44 | 404.7 |
| S@NPC-700 | 5.372 | 214.9 |
| S@NPC-750 | 6.40 | 278.2 |

**Table S4.** Comparison of rate performance of the S@NPC-700 with the recently cathodes reported for RT Na-S batteries.

| Materials | Current rate | Discharge Capacity ($mAh\ g^{-1}$) | Reference |
|---|---|---|---|
| **S@NPC-700** | **1 C/2 C** | **496/280.9** | **This work** |
| CFC/S | 1 C | 48 | S1 |
| CNT@GNR/S | 1 C | 200 | S2 |
| rGO/$VO_2$/S | 2 C | 194 | S3 |
| S@CNT/NPC | 1 C | 454 | S4 |
| VC-CNFs@S | 1C | 295 | S5 |
| NGNS/S-H25 | 2 C | 61 | S6 |
| cZIF-8/S | 2 C | 220 | S7 |
| S@C | 1 C | 440 | S8 |

## References


S1 Q. Lu, X. Wang, J. Cao, C. Chen, K. Chen, Z. Zhao, Z. Niu and J. Chen, *Energy Storage Mater.*, 2017, **8**, 77-84.

S2 A. P. Vijaya Kumar Saroja, K. Muthusamy and R. Sundara, *Adv. Mater. Interfaces*, 2019, **6**, 1801873-1801881.

S3 W. Du, Y. Wu, T. Yang, B. Guo, D. Liu, S.-J. Bao and M. Xu, *Chem. Eng. J.*, 2020, **379**, 122359-122365.

S4 T. Yang, W. Gao, B. Guo, R. Zhan, Q. Xu, H. He, S.-J. Bao, X. Li, Y. Chen and M. Xu, *J. Mater. Chem. A*, 2019, **7**, 150-156.

S5 W. Tang, W. Zhong, Y. Wu, Y. Qi, B. Guo, D. Liu, S.-J. Bao and M. Xu, *Chem. Eng. J.*, 2020, **395**, 124978.

S6 Y. Hao, X. Li, X. Sun and C. Wang, *Chemistry Select*, 2017, **2**, 9425-9432.

S7 Y.-M. Chen, W. Liang, S. Li, F. Zou, S. M. Bhaway, Z. Qiang, M. Gao, B. D. Vogt and Y. Zhu, *J. Mater. Chem. A*, 2016, **4**, 12471-12478.

S8 R. Carter, L. Oakes, A. Douglas, N. Muralidharan, A. P. Cohn and C. L. Pint, *Nano Lett.*, 2017, **17**, 1863-1869.

S9 F. Nitze, K. Fossum, S. Xiong, A. Matic and A.E.C. Palmqvist, *J. Power Sources,* 2016, **317**, 112-119.

S10 Q. Pang, J. Tang, H. Huang, X. Liang, C. Hart, K.C. Tam and L.F. Nazar, *Adv. Mater.*, 2015, **27**, 6021-6028.

S11 W. Chong, J. Huang, Z. Xu, X. Qin, X. Wang and J. Kim, *Adv. Funct. Mater.*, 2017, **27**, 1604815

S12 L. Zeng, Y. Yao, J. Shi, Y. Jiang, W. Li, L. Gu and Y. Yu, *Energy Storage Mater.*, 2016, **5**, 50-57.